J Electroceram (2006) 16:199–205
DOI 10.1007/s10832-006-6362-9

Ni-Cu-Zn Ferrites for low temperature firing: II. Effects of powder morphology and Bi_2O_3 addition on microstructure and permeability

J. Mürbe · J. Töpfer

Received: 7 July 2005 / Revised: 7 July 2005 / Accepted: 28 November 2005

Abstract The morphology of Ni-Cu-Zn ferrite powders obtained by milling of a calcined raw materials mixture strongly effects the densification behavior during sintering at 900°C. In order to obtain dense samples sub-micron powders with enhanced reactivity are required. The addition of Bi_2O_3 as sintering additive is beneficial: the density of samples sintered at 900°C increases with the bismuth oxide concentration up to 0.75 wt.%. The process of liquid phase sintering was studied by dilatometry. The grain size of the sintered samples slightly increases for 0.25 wt.% Bi_2O_3 compared to bismuth-free samples, whereas for 0.3–0.5 wt.% Bi_2O_3 additions bimodal grain growth is observed with a significant fraction of very large grains. For >0.5 wt.% Bi_2O_3 a homogeneous coarse-grained microstructure is obtained. The permeability increases for small bismuth oxide additions, but decreases for a Bi-oxide content of more than 0.5%. Maximum permeability of $\mu_i = 900$ is observed for intermediate Bi_2O_3 concentrations.

PACS codes: 75.50 Gg; 81.20 Ev; 81.40 Rs

Keywords Soft ferrites · Ni-Cu-Zn ferrites · High permeability · Powder morphology

1. Introduction

Ni-Cu-Zn ferrites are soft magnetic materials that are used for inductive multilayer devices because of their low sintering temperature and their good performance at intermediate to high frequencies. Ni-Cu-Zn ferrites are co-fired with internal Ag conductors; because of the melting point of silver the sintering temperature is limited to $T \leq 950$°C. The first multilayer chip inductors were developed two decades ago [1, 2]. Multilayer chip LC filters and hybrid circuit devices appeared as second generation of inductive multilayer SMD components [3].

The effect of ferrite composition on the sintering behavior and permeability characteristics has been studied in detail recently [4]; to guarantee effective sintering at low temperature ($T \leq 950$°C) and provide sufficient permeability and inductance the optimum Ni-Cu-Zn ferrite has a Cu-content of about $y = 0.2$ in $Ni_{1-x-y}Cu_yZn_xFe_2O_4$ (with $x = 0.4$–0.6) and a small Fe deficiency, e.g. $Ni_{0.20}Cu_{0.20}Zn_{0.60+z}Fe_{2-z}O_{4-(z/2)}$ with $z \approx 0.02$.

Because of the required low sintering temperature it is crucial to use ferrite powders with high sintering activity at 900°C. This can be realized by two main routes: (i) preparation of powders with small particles and high surface energy or (ii) addition of sintering additives. Several soft-chemistry routes have been explored in order to synthesize reactive powders, e.g. sol-gel synthesis [5], auto-combustion synthesis [6] or co-precipitation of oxalates [7]. Different sintering additives have been proposed to enhance the densification behavior of Ni-Cu-Zn ferrites, e.g. V_2O_5 [8], PbO [9] and glasses [10]. Bismuth oxide has frequently been used to improve the low-temperature densification of Ni-Cu-Zn ferrites [11–13]. Using less than 1 wt.% of Bi_2O_3 as sintering additive we obtained ferrites with a permeability of $\mu = 900$ after sintering at 900°C [14]. Very recently, Jeong et al. [15] also described the role of Bi_2O_3 addition for the preparation of high-permeability Ni-Cu-Zn ferrites.

In this contribution we report on the preparation of highly reactive sub-micron Ni-Cu-Zn ferrite powders by milling of the calcined raw materials. The influence of powder particle

J. Mürbe · J. Töpfer (✉)
Fachhochschule Jena, FB Werkstofftechnik,
Carl-Zeiss-Promenade 2, 07745 Jena, Germany
e-mail: joerg.toepfer@fh-jena.de

size and bismuth oxide addition on the densification behavior, ferrite microstructure and permeability will be outlined. It is shown that, contrary to other studies [15], at intermediate concentrations of Bi_2O_3 (0.3–0.5 wt.%) an inhomogeneous microstructure with large grains is formed causing maximum permeability.

2. Experimental

Ferrite powders of composition $(NiO)_{0.20}(ZnO)_{0.62}(CuO)_{0.20}(Fe_2O_3)_{0.99}$ were prepared by the ceramic route. Iron oxide (TKS Germany, grade HP) with a specific surface $S = 4.3$ m^2/g; NiO (Inco, Black Nickel Oxide, Grade F) with $S = 70$ m^2/g; CuO p. A. (Merck) with $S = 4.6$ m^2/g and ZnO (Harzsiegel Heubach, Germany, standard grade) with $S = 4.5$ m^2/g were used as starting materials. The oxides were wet mixed for 12 h in a polyethylene container. After drying the powder was calcined at 750°C for 2 h. Next, Bi_2O_3 was added (0, 0.25, 0.375, 0.5, 0.75 and 1 wt.%) and the powder was wet milled in a planetary ball mill. The powder was compacted using polyvinyl-alcohol as binder to give pellets for sintering studies or toroids for permeability measurements.

The phase formation was evaluated with X-ray powder diffractometry (Siemens D5000). The particle size was measured with laser diffraction (Malvern Mastersizer 2000) and the bulk density of sintered samples was determined from the dimensions and weight. Shrinkage of cylindrical samples during sintering was studied with a NETSCH DIL402 dilatometer (heating to 1000°C with 4 K/min). The microstructure of sintered pellets was evaluated with scanning and transmission electron microscopes (Zeiss DSM940A and Philips CM20T). The permeability of the sintered toroids (13 mm outer diameter, 6.5 mm inner diameter, 3 mm thickness) was measured with an impedance analyzer from 1 to 1000 kHz. For frequencies of up to 2 GHz permeability measurements were performed using an Agilent E4991A impedance/materials analyzer.

3. Results and discussion

3.1. Powder preparation

The mixed raw materials were calcined at temperatures from 600–800°C. In order to identify the optimum calcination temperature, i.e. for complete spinel formation and only little particle growth, the phase formation has been investigated with XRD (Fig. 1). In agreement with earlier studies by Byeon et al. [16], at $T < 700$°C traces of the starting oxides were detected; therefore calcination was performed at 750°C. The calcined powder was wet milled for several hours (Fig. 2); after 4 h of milling a mean particle size of $d_{50} = 0.5$–$0.6\ \mu$m has been reached. The powder morphology after calcination and wet milling is shown in Fig. 3. The wet-milled sub-micron powder has a specific surface of about 14 m^2/g.

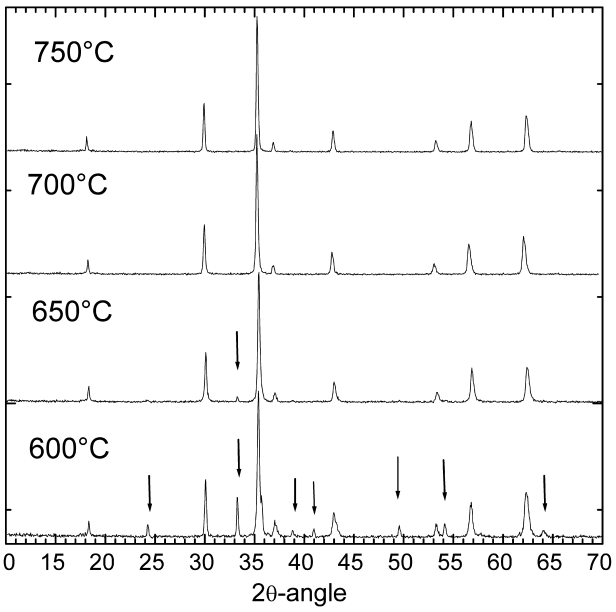

Fig. 1 XRD Plots of powders calcined at temperatures of 600, 650, 700 and 750°C (arrows mark peaks of non-reacted starting oxides)

3.2. Sintering without additives

The density of powder compacts sintered at 900°C for 30 min or 2 h as a function of the particle size of the ferrite powder is shown in Fig. 4. The density of the sintered samples increases with decreasing powder particle size; a substantial density enhancement is observed for sub-micron powders. For a powder with $d_{50} = 0.5\ \mu$m a density of 5 g/cm^3 is

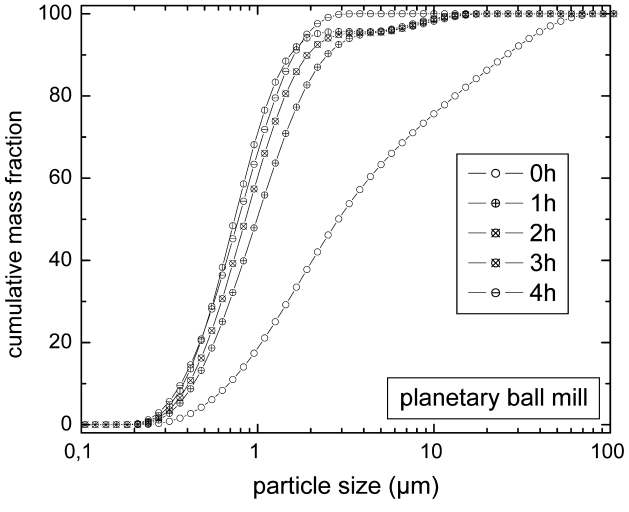

Fig. 2 Particle size distribution of ferrite powders calcined at 750°C during wet milling

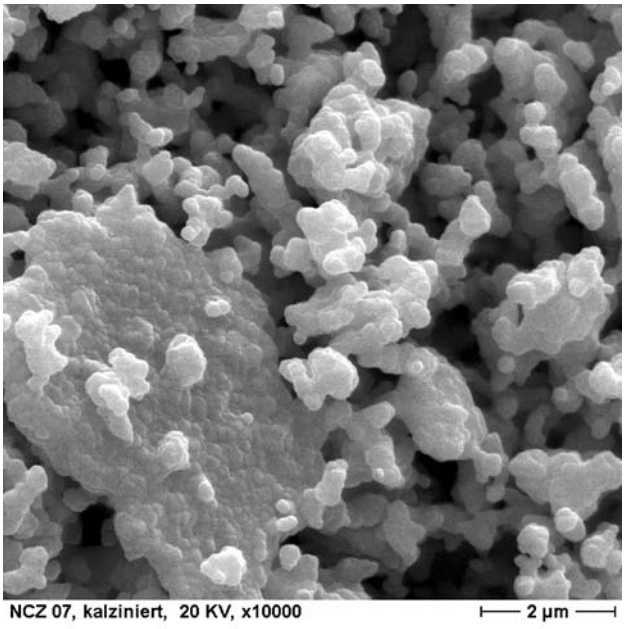

(a)

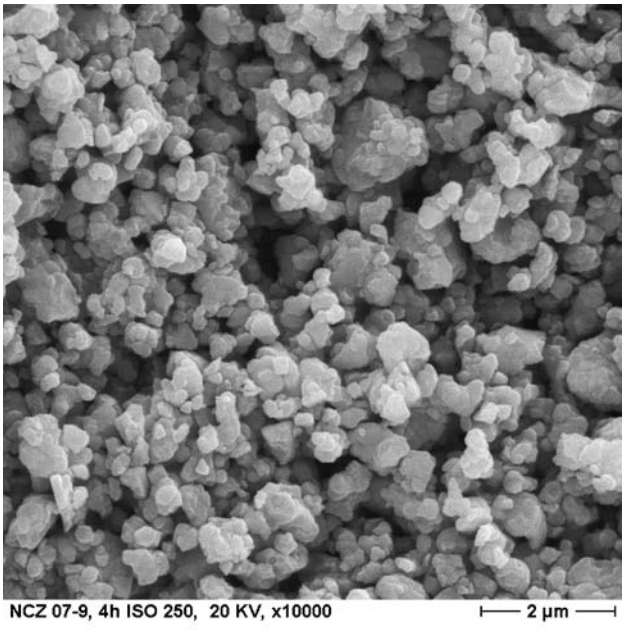

(b)

Fig. 3 SEM micrographs of ferrite powders after calcination at 750°C (a) and after 4 h of wet milling (b)

obtained after sintering at 900°C for 30 min. Sintering for 2 h at 900°C gives the same trend. For powders with $d_{50} > 1\ \mu$m the density increases by prolonged sintering at 900°C, but a sinter density of $\geq$5 g/cm^3 generally requires sub-micron powders with a $d_{50} = 0.5$–$0.6\ \mu$m. The increased sintering activity of sub-micron powders is also reflected in shrinkage curves (Fig. 5) of compacts made from powders of different particle size. The onset of sintering is reduced from 750°C to 700°C for powders with a d_{50} of 2 and 0.5 μm, respectively. The main shrinkage of the sub-micron powder

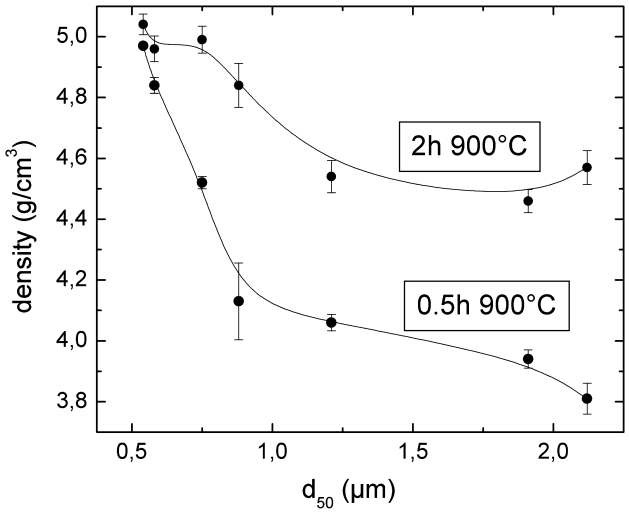

Fig. 4 Density of samples sintered at 900°C as function of the powder particle size

appears at lower temperature; the shrinkage rate has a maximum at 900°C. Whereas a coarse powder with $d_{50} = 2\ \mu$m shows a broad shrinkage rate peak, for sub-micron powders this peak appears to be much sharper and intense signaling enhanced reactivity.

3.3. Sintering with bismuth oxide additions

The addition of bismuth oxide generally increases the density of samples sintered at 900°C. For a powder ball-milled down to $d_{50} = 1.6\ \mu$m the addition of bismuth oxide significantly enhances the density (Fig. 6), but the maximum density is limited to about 5.05 g/cm^3. In the case of a sub-micron powder (with a sinter density of 5 cm^3/g after 2 h at 900°C already observed without sintering aid) the addition of Bi_2O_3

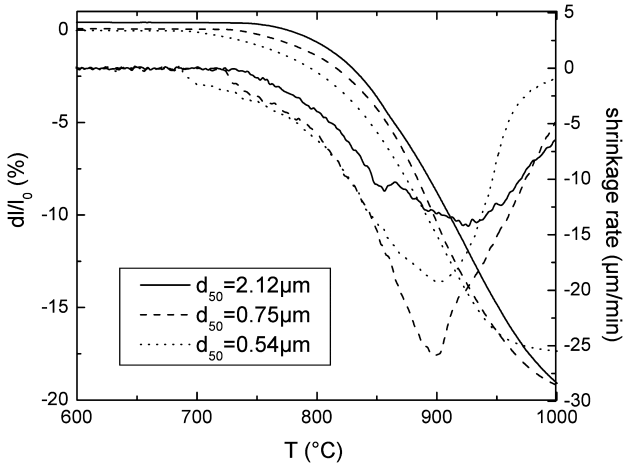

Fig. 5 Relative shrinkage and shrinkage rate of compacts made from ferrite powders of different particle size without sintering additive, (heating rate 4 K/min)

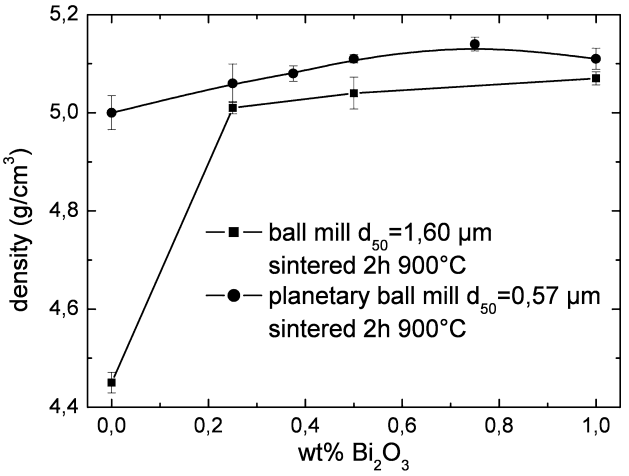

Fig. 6 Density of samples sintered at 900°C as function of the Bi_2O_3 concentration (mean particle size of the powders: $d_{50} = 0.57$ and 1.60 μm)

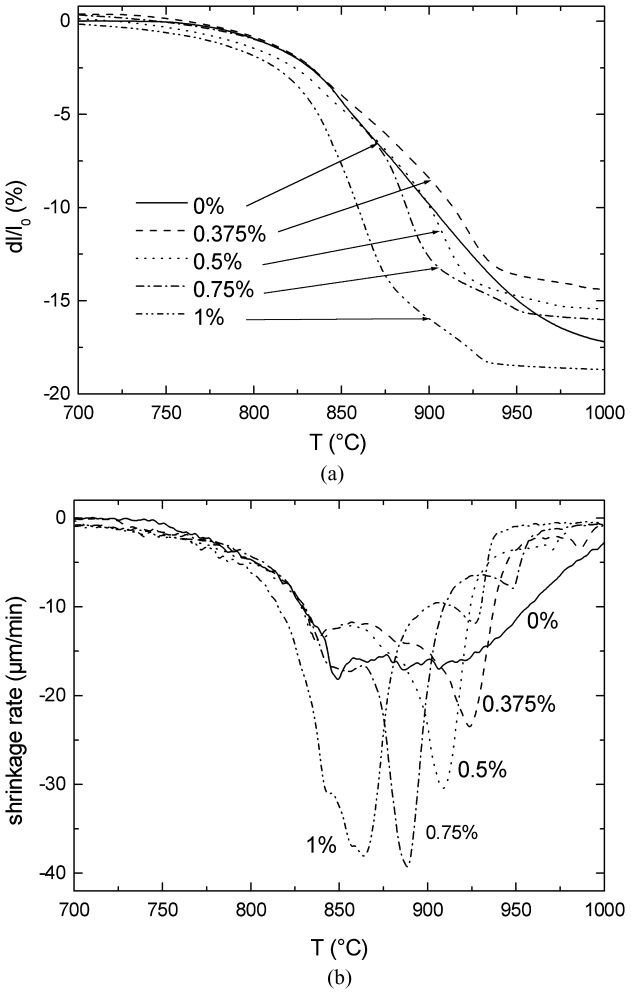

Fig. 7 Relative shrinkage (a) and shrinkage rate (b) during heating to 1000°C of compacts made from ferrite powders with $d_{50} = 0.57$ μm as a function of Bi_2O_3 concentration (heating rate 4 K/min)

further improves the densification and a maximum density of 5.15 g/cm^3 is obtained for 0.75 wt.% Bi_2O_3 addition.

The shrinkage curves of samples made from sub-micron ferrite powders with different amounts of sintering additive reveal a change in the sintering process and the underlying mechanism. The addition of bismuth oxide shifts the maximum shrinkage down to lower temperature. Moreover, whereas for the sample without bismuth oxide a more or less smooth shrinkage curve is observed, all samples with Bi_2O_3 addition display shrinkage curves with several kinks (Fig. 7(a)). These features are also reflected in the shrinkage rate plots (Fig. 7(b)): a bismuth free sample has a very broad maximum shrinkage rate, whereas bismuth-containing samples show quite sharp shrinkage rate peaks. A closer inspection of the curves reveals a number of individual shrinkage rate peaks with the temperature of most of the peaks changing with bismuth oxide concentration. Significant shrinkage starts at about 770–800°C signaling the onset of the liquid phase formation (lowest eutectic in the systems Bi_2O_3-CuO-NiO-ZnO-Fe_2O_3). All samples show a small shrinkage rate peak (or shoulder) at about 830–850°sC close to the melting point of Bi_2O_3 (825°C). The maximum shrinkage rate peak is shifted from 925 to 860°C for 0.375 and 1 wt.% Bi_2O_3, respectively. A third small peak is also systematically shifted from 980 to 925°C for 0.375 and 1 wt.% Bi_2O_3, respectively. This series of shrinkage rate peaks is a signature of the underlying liquid phase sintering, i.e. liquid formation, rearrangement and densification. The last two processes proceed at lower temperature if the amount of liquid phase increases.

3.4. Microstructure and permeability of sintered ferrites

The microstructures of compacts made from a reactive submicron powder ($d_{50} = 0.57$ μm) with various amounts of Bi_2O_3 and sintered at 900°C for 2 h are shown as SEM micrographs in Fig. 8. While for a Bi-free sample a fine-grained microstructure with an average grain size of about 1 μm is observed, only little grain growth occurs if 0.25 wt.% Bi_2O_3 are added. At intermediate Bi_2O_3 concentrations (0.3–0.5 wt.%) a bimodal, inhomogeneous microstructure evolves: small grains of size of about 1 μm are located between regions of large grains of 20–30 μm size. The discontinuous grain growth might be indicative of an inhomogeneous distribution of the liquid phase. For 0.75 and 1 wt.% Bi_2O_3 the microstructure is characterized by a more homogeneous grain size distribution with gains of 10–15 μm in size.

High-rsesolution TEM micrographs of a Bi-free sample display very thin boundaries between the grains with a dihedral angle of 120° which is consistent with an equilibrium situation of a polycrystalline single-phase microstructure (Fig. 9(a)). In contrast, for a sample with 0.375 wt.% Bi_2O_3 (sintered 2 h at 900°C) two typical morphologies

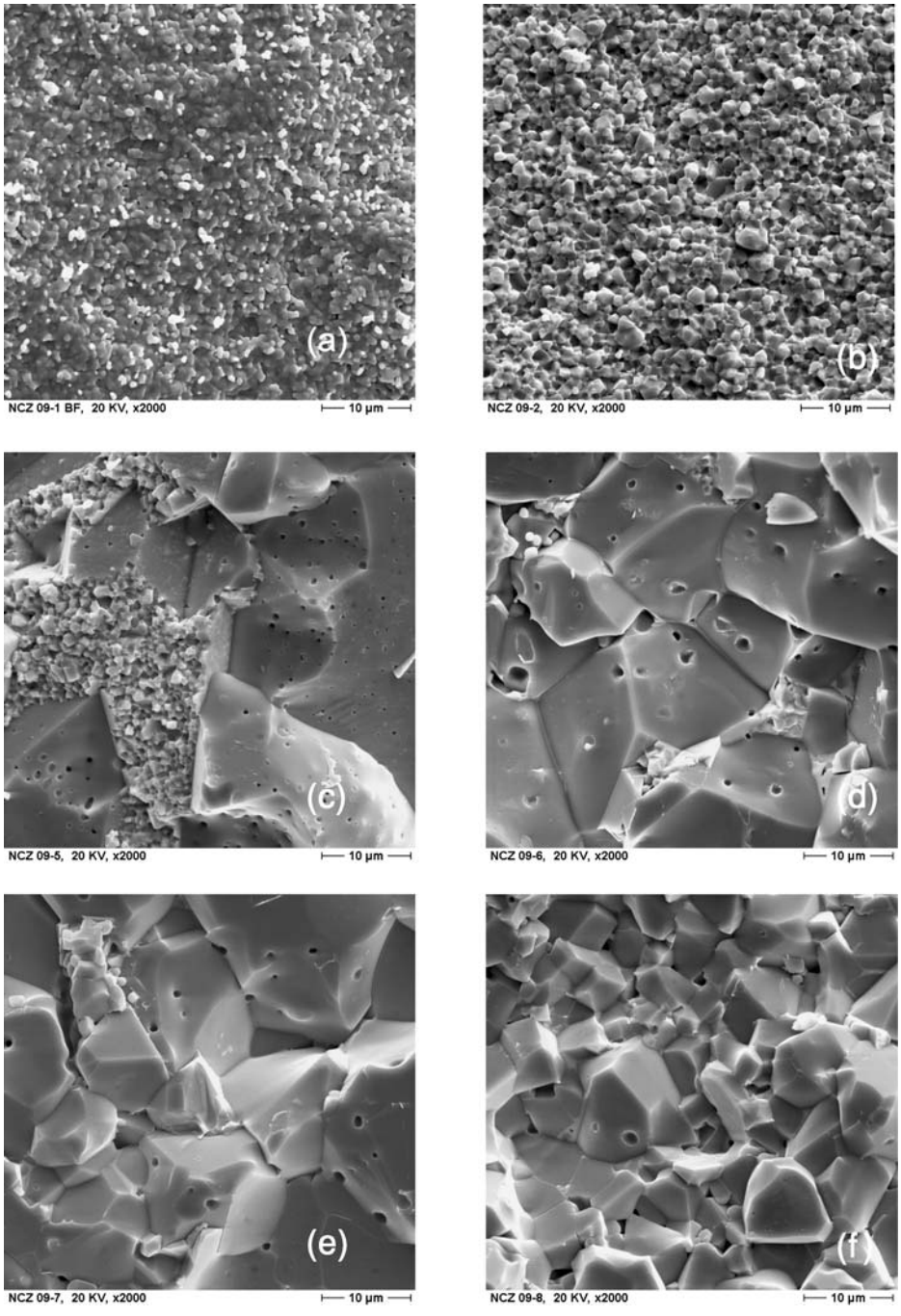

Fig. 8 SEM Micrographs of ferrites sintered at 900°C for 2 h with 0 wt.% (a), 0.25 wt.% (b), 0.375 wt.% (c), 0.5 wt.% (d), 0.75 wt.% (e) and 1 wt.% (f) Bi_2O_3

are observed: (i) continuous, amorphous boundary layers of thickness of 7–9 nm between neighboring large ferrite grains with amorphous three grain junctions; the dihedral angle of about 60° indicates a continuous second phase film between the grains (Fig. 9(b)) and (ii) regions of smaller grains separated by a crystalline Bi_2O_3-rich intergranular phase (Fig. 9(c)). An EDX-linescan across an amorphous grain boundary phase between two large ferrite grains of situation (i) clearly demonstrates that the concentrations of the ferrite main constituents are strongly reduced (signals only shown here for Ni and Cu), whereas an increase of the Bi-signal in the boundary region is observed (Fig. 9(d)).

The permeability of samples sintered at 900°C is strongly related to the ceramic microstructure and hence to the amount of Bi_2O_3 addition. Starting with a permeability at 1 MHz of about 580 for a Bi-free sample with 1 μm large grains, the permeability increases with Bi_2O_3 concentration and reaches a maximum of about $\mu = 890$ at 0.375–0.5 wt.% Bi_2O_3 (Fig. 10); larger additive concentrations lead to a decline of permeability. The result of a $\mu = 890$ is a much higher

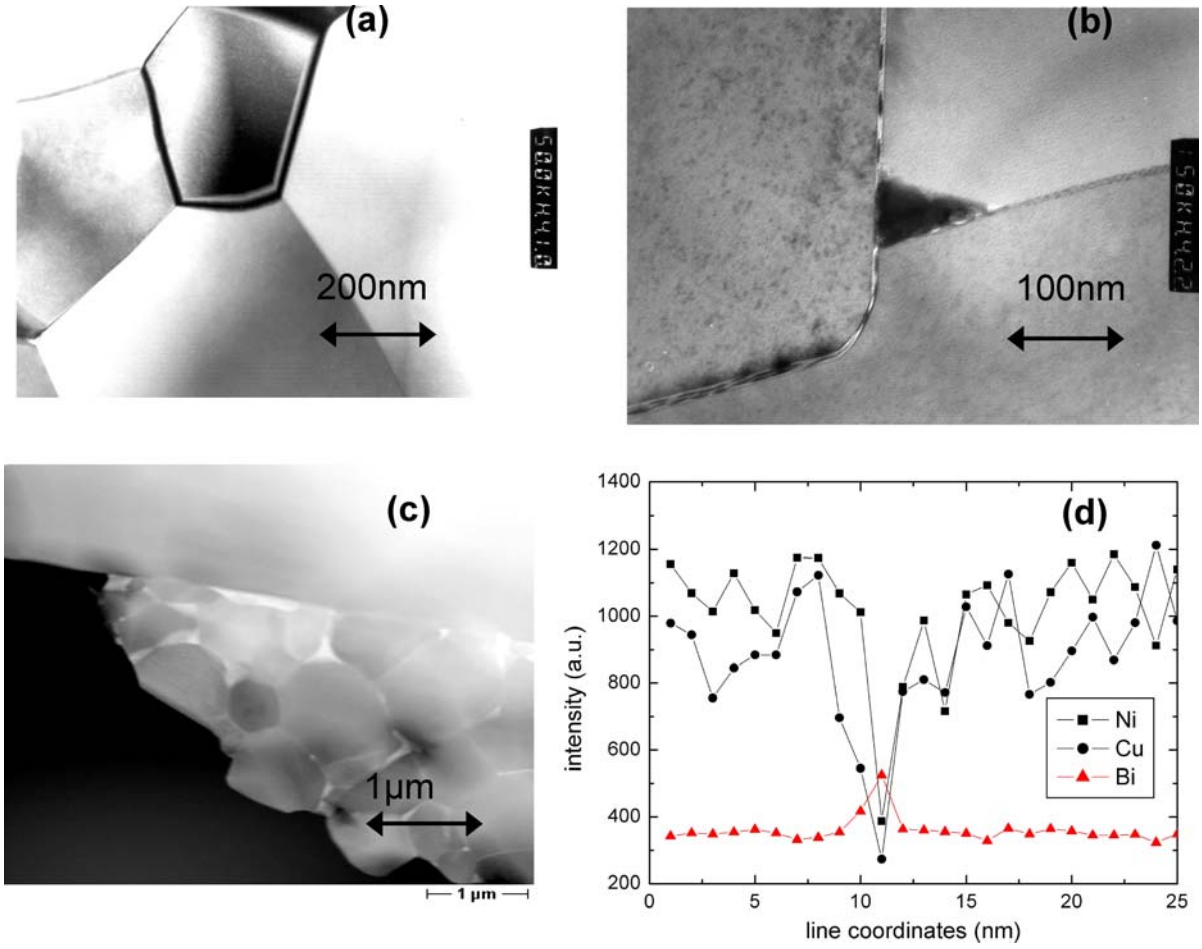

Fig. 9 TEM Micrographs of ferrites sintered at 900°C for 2 h with 0 wt.% (a) and 0.375 wt.% Bi_2O_3 (b, c); and EDX profile across a phase boundary of sample (b)

permeability than previously reported by other authors; e.g. Jean et al. [12] obtained a maximum permeability of about 140 with 2 wt.% Bi_2O_3. Jeong et al. [15] recently also observed a variation of permeability with Bi_2O_3 additive concentration, but, contrary to our results, these authors found a maximum permeability of $\mu = 880$ at 0.25 wt.% Bi_2O_3 with a fine-grained (2 μm) microstructure.

The relation between permeability and grain size has been a central foscus of ferrite research for many years. In the domain wall displacement model originally developed by Globus the static permeability has been shown to be proportional to the grain size [17]. For smaller, single-domain particles the rotational permeability is the main contribution to the total permeability. The nonmagnetic grain boundary model has been developed to explain the grain size dependence of μ [18, 19]. By analyzing the complex permeability spectra of Ni-Cu-Zn ferrites Nakamura [20] concluded that both domain wall displacement and spin rotation contribute to the permeability at a frequency below 10 MHz.

We interpret the large permeability at intermediate amounts of Bi_2O_3 additive as being linked to the appearance of large grains in those samples. Domain wall displacement is becoming more easily performed leading to high permeability. Large ferrite grains of size of about 25–30 μm, as obtained by sintering at 900°C with a Bi_2O_3 addition of 0.3–0.5 wt.%, are very beneficial for dense Ni-Cu-Zn ferrites with large permeability.

4. Conclusions

Ni-Cu-Zn ferrites prepared from reactive sub-micron powders sinter to high density at 900°C. The addition of Bi_2O_3 further enhances the densification and has a dramatic influence of the microstructure and permeability of the sintered samples. With the addition of 0.35–0.5 wt.% Bi_2O_3 a bimodal microstructure with large (25–30 μm) grains surrounded by small-grained (1–2 μm) regions is observed. These ferrites have a permeability of about 900 after sintering at 900°C and are basic materials for monolithic or embedded multilayer inductors.

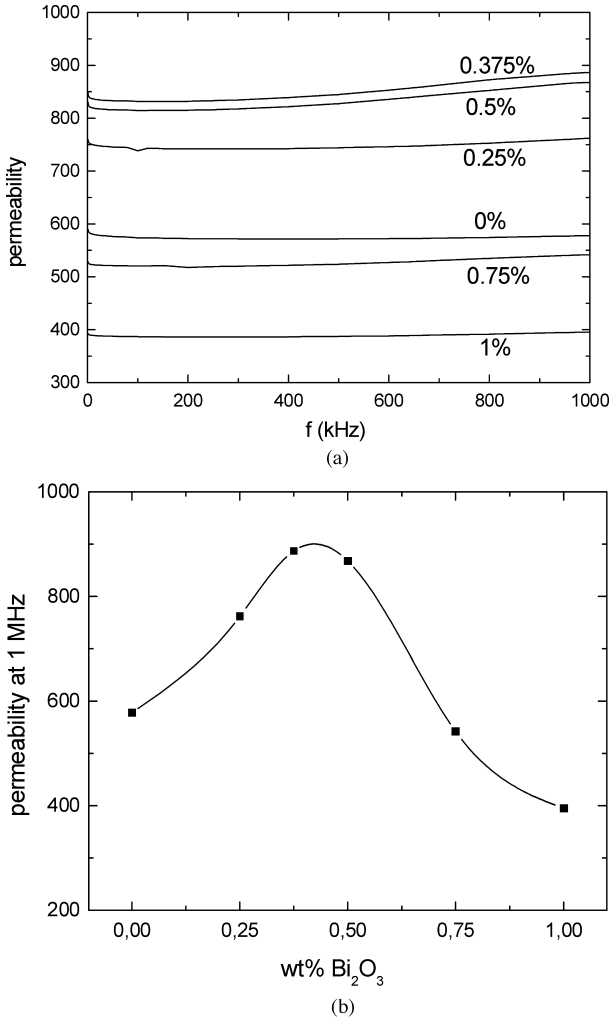

Fig. 10 Permeability of samples sintered at 2 h for 900°C versus frequency for different Bi_2O_3 concentrations (a), and μ at 1 MHz as function of Bi_2O_3 concentration (b)

Acknowledgments The authors thank the Bundesministerium für Bildung und Forschung (Germany) for financial support (grant 03WKF03A). We acknowledge the contributions of Mrs. M. Friedrich (FHJ) for SEM, Mr. V. Döhnel (Tridelta GmbH) for some permeability measurements and Drs. D. Hesse and S. Senz (MPI Halle) for TEM investigations.

References

1. T. Nomura and A. Nakano, Proceedings of the Sixth International Conference on Ferrites (ICF6), (Tokyo, 1992), p. 1198.
2. T. Nakamura and Y. Okano, *J. Phys. IV France*, **7**, C1–91 (1997).
3. K. Yasuda, Y. Mochizuki, and M. Takaya, Proceedings of the Eight International Conference of Ferrites (ICF8), (Kyoto, 2000), p. 1162.
4. J. Mürbe and J. Töpfer, *J. Electroceramics*, **15**, 215–221 (2005).
5. K.O. Low and F.R. Sale, *J. Magn. Magn. Mater.*, **30**, 246 (2002).
6. Z. Yue, J. Zhou, L. Li, H. Zhang, and Z. Gui, *J. Magn. Magn. Mater.*, **208**, 55–60 (2000).
7. J. Töpfer and J. Mürbe, Proceedings of the Ninth International Conference of Ferrites (ICF9), (San Francisco, 2004), p. 885.
8. J.Y. Hsu, W.S. Ko, and C.J. Chen, *IEEE Trans. Magn.*, **31**, 3994 (1995).
9. J.H. Jean and C.H. Lee, *J. Am. Ceram. Soc.*, **82**, 343 (1999).
10. Y.-R. Wang and S.-F. Wang, *Intl. J. Inorgan. Mater.*, **3**, 1189–1192 (2001).
11. J.-Y. Hsu, W.-S. Ko, H.-D. Shen, and C.-J. Chen, *IEEE Trans. Magn.*, **30**, 4875–77 (1994).
12. J.H. Jean and C.-H. Lee, *Jpn. J. Appl. Phys.*, **38**, 3508–3512 (1999).
13. S.F. Wang, Y.R. Wang, T. Yang, C.F. Chen, C.A. Lu, and C.Y. Huang, *J. Magn. Magn. Mater.*, **220**, 129–138 (2000).
14. J. Töpfer, J. Mürbe, S. Barth, E. Müller, and F. Bechtold, *Key Engin. Mater.*, **264–268**, 1233–36 (2004).
15. J. Jeong, Y.H. Han, and B.C. Moon, *J. Mater. Sci: Mater. Electronics*, **15**, 303–306 (2004).
16. S.C. Byeon, H.J. Je, and K.S. Hong, *Jpn. J. Appl. Phys.*, **36**, 5103–5108 (1997).
17. R. Lebourgeois, C. Le Fur, M. Pate, and J.P. Ganne, *J. Magn. Magn. Mater.*, **160**, 329–332 (1996).
18. M.T. Johnson and E.G. Wisser, *IEEE Trans. Magn.*, **26**, 1987–1989 (1990).
19. P.J. van der Zaag, J.J.M. Ruigrok, A. Noordermeer, M. van Delden, P.T. Por, M.T. Rekveldt, D.M. Donnet, and J.N. Chapman, *J. Appl. Phys.*, **74**, 4085–4095 (1993).
20. T. Nakamura, *J. Magn. Magn. Mater.*, **168**, 285–291 (1997).